



# Integrated PET/MRI scanner with oxygen-15 labeled gases for quantification of cerebral blood flow, cerebral blood volume, cerebral oxygen extraction fraction and cerebral metabolic rate of oxygen

Hiroshi Ito<sup>1,2</sup> · Hitoshi Kubo<sup>2</sup> · Kazuhiro Takahashi<sup>2</sup> · Ken-Ichi Nishijima<sup>2</sup> · Naoyuki Ukon<sup>2</sup> · Ayaka Nemoto<sup>2</sup> · Shigeyasu Sugawara<sup>1,2</sup> · Ryo Yamakuni<sup>1</sup> · Masanobu Ibaraki<sup>3</sup> · Shiro Ishii<sup>1</sup>

Received: 25 October 2020 / Accepted: 4 January 2021 / Published online: 27 January 2021  
© The Japanese Society of Nuclear Medicine 2021

## Abstract

**Objectives** Measurement of cerebral blood flow (CBF), cerebral blood volume (CBV), cerebral oxygen extraction fraction (OEF) and cerebral metabolic rate of oxygen (CMRO<sub>2</sub>) by PET with oxygen-15 labeled gases is useful for diagnosis and treatment planning in cases of chronic occlusive cerebrovascular disease. In the present study, CBF, CBV, OEF and CMRO<sub>2</sub> were measured using the integrated design of PET/MRI scanner system. This is a first attempt to measure cerebral perfusion and oxygen metabolism using PET/MRI with oxygen-15 labeled gases.

**Methods** PET/MRI measurements with the steady-state method of oxygen-15 labeled gases, carbon monoxide (C<sup>15</sup>O), oxygen (<sup>15</sup>O<sub>2</sub>), and carbon dioxide (C<sup>15</sup>O<sub>2</sub>) were performed on nine healthy men. Two kinds of attenuation correction for PET were performed using MRI with Dixon sequence (DIXON) and Dixon sequence with model-based bone segmentation (DIXONbone). A real-time motion correction of PET images was also performed using simultaneously measured MR images to detect head motion.

**Results** Mean and SD values of CBF, CBV, OEF, and CMRO<sub>2</sub> in the cerebral cortices with attenuation correction by DIXON were 31 ± 4 mL/100 mL/min, 2.7 ± 0.2 mL/mL, 0.40 ± 0.07, and 2.5 ± 0.3 mL/100 mL/min without real-time motion correction, and 33 ± 4 mL/100 mL/min, 2.7 ± 0.2 mL/mL, 0.40 ± 0.07, and 2.6 ± 0.3 mL/100 mL/min with real-time motion correction, respectively. Values with of CBF, CBV, OEF, and CMRO<sub>2</sub> with attenuation correction by DIXONbone were 35 ± 5 mL/100 mL/min, 2.8 ± 0.2 mL/mL, 0.40 ± 0.07, and 2.8 ± 0.3 mL/100 mL/min without real-time motion correction, and 38 ± 5 mL/100 mL/min, 2.8 ± 0.2 mL/mL, 0.40 ± 0.07, and 3.0 ± 0.4 mL/100 mL/min with real-time motion correction, respectively.

**Conclusions** Using PET/MRI with oxygen-15 labeled gases, CBF, CBV, OEF, and CMRO<sub>2</sub> could be measured. Values of CBF, CBV, and CMRO<sub>2</sub> measured with attenuation correction by DIXON were significantly lower than those measured with correction by DIXONbone. One of the reasons for this is that attenuation correction of DIXON does not take into consideration of the photon absorption by bone. OEF values, corresponding to ratios of CMRO<sub>2</sub> to CBF, were not affected by attenuation correction methods. Values of CBF and CMRO<sub>2</sub> with a real-time motion correction were significantly higher than those without correction. Using PET/MRI with adequate corrections, similar values of CBF, CBV, OEF, and CMRO<sub>2</sub> as PET alone scanner system reported previously were obtained.

**Trial registration** The UMIN clinical trial number: UMIN000033382.

**Keywords** PET/MRI · CBF · CMRO<sub>2</sub> · Oxygen-15 · Brain

## Introduction

Measurement of cerebral blood flow (CBF), cerebral blood volume (CBV), cerebral oxygen extraction fraction (OEF), and cerebral metabolic rate of oxygen (CMRO<sub>2</sub>) by

✉ Hiroshi Ito  
h-ito@fmu.ac.jp

Extended author information available on the last page of the article

positron emission tomography (PET) with  $^{15}\text{O}$ -labeled carbon dioxide ( $\text{C}^{15}\text{O}_2$ ),  $^{15}\text{O}$ -labeled carbon monoxide ( $\text{C}^{15}\text{O}$ ), or  $^{15}\text{O}$ -labeled oxygen ( $^{15}\text{O}_2$ ) is widely used for investigation into the pathophysiology of several brain diseases, especially occlusive cerebrovascular disease [1–7]. Decreased cerebral perfusion pressure due to major cerebral arterial occlusive disease causes cerebral autoregulatory vasodilatation for maintenance of CBF (stage I hemodynamic change). Decreased cerebral perfusion pressure below the lower limit of cerebral autoregulation causes a decrease in CBF with an increase in OEF, for maintenance of  $\text{CMRO}_2$  (stage II hemodynamic change). For the assessment of stage I hemodynamic compromise, measurements of CBF at rest and during acetazolamide stress by PET or single photon emission tomography (SPECT) are widely performed [8, 9]. Stage II hemodynamic compromise, however, can be assessed by measuring OEF, which can be done only by PET [10].

The integrated design of the positron emission tomography/magnetic resonance imaging (PET/MRI) scanner system allows simultaneous data acquisition for PET and MRI [11], and therefore, it must have potential for clinical and research settings of neurological and psychiatric diseases including cerebrovascular diseases [12, 13]. Such PET/MRI scanner system can be applied for correction of partial volume effects, motion correction, and determination of image-derived input function of brain PET [12].

In the present study, CBF, CBV, OEF and  $\text{CMRO}_2$  were measured using the integrated design of the PET/MRI scanner system and  $^{15}\text{O}$ -labeled gases with two kinds of attenuation corrections for PET by MRI. A real-time head motion correction of PET images using MR images simultaneously measured with PET was also applied. Values of CBF, CBV, OEF, and  $\text{CMRO}_2$  with two kinds of attenuation correction for PET with and without a real-time motion correction were compared. This is a first attempt to measure cerebral perfusion and oxygen metabolism using PET/MRI with  $^{15}\text{O}$ -labeled gases.

## Materials and methods

### Subjects

Nine healthy men (20–27 years old) were recruited. No subject had notable organic lesions in the brain according to MRI. The subjects were free of somatic, neurological and psychiatric disorders on the basis of their medical history. They were free from medications having central nervous action. The study was approved by the Institutional Review Board of the Fukushima Medical University, Fukushima, Japan. Written informed consent was obtained from all subjects.

### PET/MRI experimental procedure

All PET studies were performed with a Siemens mMR PET/MRI scanner, which provides 127 sections with an axial field of view of 25.8 cm [14]. The intrinsic spatial resolution was 4.3 mm in-plane and 4.3 mm full-width at half maximum (FWHM) axially. Data were acquired in three-dimensional mode. Scatter was corrected [15]. PET measurements with the steady-state method of  $^{15}\text{O}$ -labeled gases,  $\text{C}^{15}\text{O}$ ,  $^{15}\text{O}_2$ , and  $\text{C}^{15}\text{O}_2$  were performed on all subjects [16, 17]. Static PET scanning was started 3 min after 1 min of continuous inhalation of  $\text{C}^{15}\text{O}$  gas (a total of approximately 3 GBq supplied by mouth). Scanning time was 4 min. Then, static PET scanning was performed during inhalation of  $^{15}\text{O}_2$  gas after equilibrium had been reached and confirmed by the head radioactivity curve (a total of approximately 8.4 GBq supplied by mouth). Scanning time was 10 min, and the time from the beginning of inhalation to the beginning of scanning was 10 min. Static PET scanning was performed during inhalation of  $\text{C}^{15}\text{O}_2$  gas using the same protocol as with  $^{15}\text{O}_2$  gas (a total of approximately 2.8 GBq supplied by mouth). During each PET scanning, arterial blood sampling was performed to measure the radioactivity concentration in the blood and plasma. Arterial blood gases were also measured. For the arterial blood sampling, non-magnetic medical devices, such as a plastic needle and plastic syringe were used. Total oxygen content in arterial blood was estimated from  $\text{P}_a\text{O}_2$ , pH and hemoglobin concentration (Hb) [17].

All MRI studies were performed with a Siemens mMR PET/MRI scanner, equipped with a 3.0-T MR scanner, during and between PET scanning. Dixon sequence (DIXON) (3D-VIBE (volumetric interpolated breath-hold examination), TR: 3.56 ms, TE: 1.23 ms and 2.46 ms; field of view: 500 mm, slice thickness: 3.12 mm, resolution:  $2.6 \times 2.6 \times 3.1$  mm, 1 slab: 128 slices) and Dixon sequence with model-based bone segmentation (DIXONbone) were performed for attenuation correction of PET [18, 19]. The MR images with gradient echo-type echo planar imaging (2D GR-EPI) sequence (TR: 1000 ms, TE: 30 ms, flip angle  $75^\circ$ ; field of view: 240 mm, acquisition matrix size:  $64 \times 64$ , slice thickness: 3.0 mm, slice gap: 1.5 mm, 15 slices) to detect head motion were simultaneously measured with PET scanning for a real-time motion correction of PET images [20, 21]. Three-dimensional volumetric T1-weighted images (T1WI) and T2-weighted images (T2WI), diffusion-tensor images, arterial spin labelling images, and MR angiography were also acquired. In the present study, T1WI (three-dimensional MPRAGE magnetization prepared rapid acquisition with gradient echo sequence, TR: 1800 ms, TE: 1.98 ms, flip angle  $9^\circ$ ; field of view: 250 mm, acquisition matrix size:  $256 \times 256$ , slice thickness: 1.0 mm) were used for analyses.

Image reconstruction of PET was carried out by the ordered-subset expectation maximization (OSEM) algorithm (iterations: 3, subsets: 21) with postreconstruction Gaussian filter of 5 mm FWHM. Two attenuation corrections for PET using DIXON and DIXONbone were applied. A real-time motion correction of PET images was also applied using simultaneously measured MR images with GR-EPI sequence.

### Calculation of parametric images

Using reconstructed PET images, the radioactivity concentration in arterial blood and plasma, and arterial blood gases data, the parametric images of CBF, CBV, OEF and  $CMRO_2$  were calculated [16]. The parametric images were calculated for attenuation correction by DIXON and DIXONbone with and without real-time motion correction.

### Data analysis

Regions of interest (ROIs) were drawn on all PET images, referring to T1WI. Circular ROIs (10 mm in diameter) were defined for the cerebellar cortex, pons, thalamus, putamen, centrum semiovale, and four neocortical regions representing the base side of the frontal cortex, lateral side of the temporal cortex, inferior parietal lobule cortex, and cuneus of the occipital cortex. The average of values of four neocortical regions were calculated as the cerebral cortices.

### Results

Figure 1 shows typical images of attenuation coefficient by DIXON and DIXONbone. In the image of attenuation coefficient by DIXONbone, the skull was depicted.

Table 1 gives mean and SD values of CBF, CBV, OEF, and  $CMRO_2$  with attenuation correction by DIXON and DIXONbone with and without real-time motion correction. Values of CBF and  $CMRO_2$  measured with attenuation correction by DIXON were significantly lower than those measured with attenuation correction by DIXONbone in all brain regions for no real-time motion correction. Values of CBV measured with attenuation correction by DIXON were also significantly lower than those measured with attenuation correction by DIXONbone in all brain regions without the cerebellum and frontal cortex. The OEF values were not affected by attenuation correction methods.

Values of CBF and  $CMRO_2$  with real-time motion correction were slightly but significantly higher than those without real-time motion correction in all brain regions for both DIXON and DIXONbone. No changes in CBV or OEF were observed between with and without real-time motion correction.

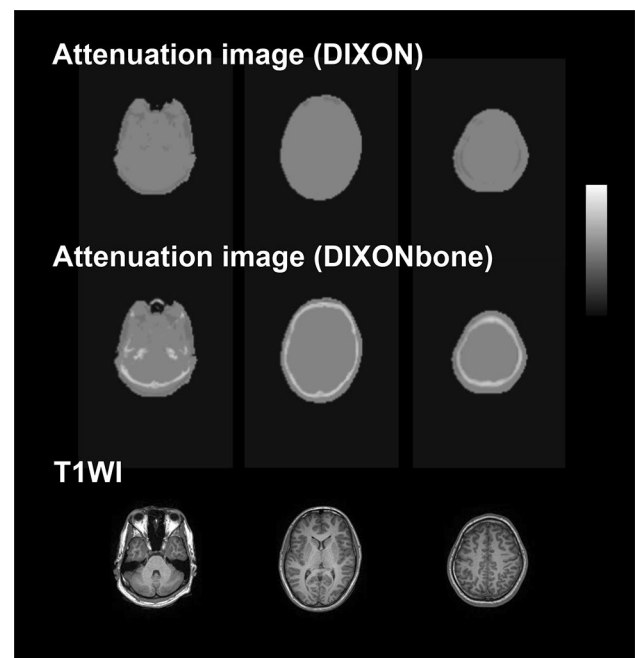


**Fig. 1** Typical images of attenuation coefficient using the Dixon sequence (DIXON) and Dixon sequence with model-based bone segmentation (DIXONbone). T1WI for the same slices of attenuation images are also shown

The coefficients of variation of CBF, CBV, OEF, and  $CMRO_2$  in the cerebral cortices were 13%, 9%, 17%, and 12%, and 13%, 9%, 17%, and 12% for attenuation correction by DIXON with and without real-time motion correction, respectively. The coefficients of variation of CBF, CBV, OEF, and  $CMRO_2$  in the cerebral cortices were 14%, 9%, 17%, and 12%, and 14%, 8%, 17%, and 13% for attenuation correction by DIXONbone with and without real-time motion correction, respectively.

Figure 2 shows the relations of CBF, CBV, OEF and  $CMRO_2$  in the cerebral cortices of each subject between values with attenuation correction by DIXON without real-time motion correction and values with attenuation correction by DIXON with real-time motion correction, or values with attenuation correction by DIXONbone with or without real-time motion correction. Significant correlations were observed in all relations.

Typical PET images of CBF, CBV, OEF, and  $CMRO_2$  with attenuation correction by DIXON and DIXONbone with and without real-time motion correction are shown in Fig. 3.

### Discussion

Using the PET/MRI scanner system with the steady-state method of  $^{15}O$ -labeled gases, CBF, CBV, OEF, and  $CMRO_2$  could be measured. Because of the PET measurement in the

**Table 1** Values of cerebral blood flow (CBF), cerebral blood volume (CBV), cerebral oxygen extraction fraction (OEF) and cerebral metabolic rate of oxygen (CMRO<sub>2</sub>)

Region	CBF	CBV	OEF	CMRO <sub>2</sub>
DIXON without motion correction				
Cerebellum	34.7 ± 3.4*	2.4 ± 0.4	0.37 ± 0.07	2.6 ± 0.4*
Pons	28.9 ± 6.1*	3.0 ± 0.6 <sup>†</sup>	0.30 ± 0.08	1.7 ± 0.4*
Thalamus	41.3 ± 4.6*	2.6 ± 0.4*	0.35 ± 0.05	2.9 ± 0.4*
Putamen	39.7 ± 6.8*	1.9 ± 0.1*	0.42 ± 0.08	3.3 ± 0.4*
Frontal cortex	31.3 ± 4.9*	2.2 ± 0.2	0.39 ± 0.07	2.5 ± 0.3*
Temporal cortex	29.0 ± 3.9*	3.0 ± 0.7*	0.38 ± 0.08 <sup>‡</sup>	2.2 ± 0.4*
Parietal cortex	32.3 ± 4.2*	2.8 ± 0.6 <sup>†</sup>	0.40 ± 0.06 <sup>‡</sup>	2.6 ± 0.4*
Occipital cortex	31.1 ± 5.3*	2.8 ± 0.3 <sup>†</sup>	0.41 ± 0.07	2.5 ± 0.3*
Centrum semiovale	13.7 ± 1.7*	1.3 ± 0.3 <sup>‡</sup>	0.38 ± 0.08	1.1 ± 0.3*
Cerebral cortices	30.9 ± 4.0*	2.7 ± 0.2*	0.40 ± 0.07 <sup>‡</sup>	2.5 ± 0.3*
DIXON with motion correction				
Cerebellum	37.4 ± 3.8 <sup>§</sup>	2.4 ± 0.4	0.37 ± 0.07	2.8 ± 0.4 <sup>§</sup>
Pons	30.4 ± 6.6 <sup>  </sup>	3.0 ± 0.6	0.30 ± 0.08	1.8 ± 0.5 <sup>  </sup>
Thalamus	44.2 ± 5.1 <sup>§</sup>	2.6 ± 0.4	0.35 ± 0.05	3.2 ± 0.5 <sup>§</sup>
Putamen	42.7 ± 7.4 <sup>§</sup>	1.9 ± 0.2	0.42 ± 0.07	3.5 ± 0.5 <sup>§</sup>
Frontal cortex	33.0 ± 5.0 <sup>§</sup>	2.2 ± 0.2	0.40 ± 0.07	2.6 ± 0.4 <sup>§</sup>
Temporal cortex	31.0 ± 4.5 <sup>§</sup>	3.0 ± 0.7	0.38 ± 0.08	2.4 ± 0.4 <sup>§</sup>
Parietal cortex	34.3 ± 4.8 <sup>§</sup>	2.8 ± 0.5	0.40 ± 0.06 <sup>  </sup>	2.8 ± 0.4 <sup>§</sup>
Occipital cortex	33.1 ± 5.6 <sup>§</sup>	2.8 ± 0.3	0.41 ± 0.07	2.7 ± 0.3 <sup>§</sup>
Centrum semiovale	14.3 ± 2.0 <sup>  </sup>	1.3 ± 0.3	0.38 ± 0.09	1.1 ± 0.3 <sup>  </sup>
Cerebral cortices	32.9 ± 4.2 <sup>§</sup>	2.7 ± 0.2	0.40 ± 0.07	2.6 ± 0.3 <sup>§</sup>
DIXONbone without motion correction				
Cerebellum	41.2 ± 4.5 <sup>**</sup>	2.4 ± 0.4	0.37 ± 0.07	3.1 ± 0.5 <sup>**</sup>
Pons	32.8 ± 6.9 <sup>††</sup>	3.1 ± 0.7	0.29 ± 0.07	1.9 ± 0.4 <sup>††</sup>
Thalamus	45.5 ± 5.3 <sup>**</sup>	2.7 ± 0.5	0.35 ± 0.05	3.2 ± 0.5 <sup>**</sup>
Putamen	44.4 ± 8.4 <sup>**</sup>	1.9 ± 0.1	0.42 ± 0.08	3.7 ± 0.5 <sup>**</sup>
Frontal cortex	37.0 ± 6.2 <sup>**</sup>	2.3 ± 0.2	0.40 ± 0.07	2.9 ± 0.4 <sup>**</sup>
Temporal cortex	32.6 ± 4.9 <sup>**</sup>	3.0 ± 0.7	0.39 ± 0.08	2.5 ± 0.5 <sup>**</sup>
Parietal cortex	36.6 ± 5.1 <sup>**</sup>	2.9 ± 0.6	0.40 ± 0.06	2.9 ± 0.4 <sup>**</sup>
Occipital cortex	35.0 ± 6.4 <sup>**</sup>	2.9 ± 0.3	0.41 ± 0.07	2.9 ± 0.3 <sup>**</sup>
Centrum semiovale	14.4 ± 1.8 <sup>††</sup>	1.3 ± 0.3	0.39 ± 0.09	1.1 ± 0.3 <sup>††</sup>
Cerebral cortices	35.3 ± 4.9 <sup>**</sup>	2.8 ± 0.2	0.40 ± 0.07	2.8 ± 0.3 <sup>**</sup>
DIXONbone with motion correction				
Cerebellum	44.9 ± 5.1	2.4 ± 0.4	0.37 ± 0.07	3.3 ± 0.5
Pons	34.6 ± 7.5	3.0 ± 0.7	0.29 ± 0.07	2.0 ± 0.5
Thalamus	49.0 ± 6.0	2.7 ± 0.5	0.35 ± 0.05	3.5 ± 0.5
Putamen	48.1 ± 9.0	1.9 ± 0.2	0.42 ± 0.07	4.0 ± 0.5
Frontal cortex	39.3 ± 6.3	2.2 ± 0.2	0.40 ± 0.07	3.1 ± 0.4
Temporal cortex	35.0 ± 5.7	3.1 ± 0.7	0.39 ± 0.08	2.7 ± 0.5
Parietal cortex	39.0 ± 5.8	2.8 ± 0.5	0.41 ± 0.06	3.2 ± 0.5
Occipital cortex	37.5 ± 6.8	2.9 ± 0.3	0.41 ± 0.07	3.1 ± 0.4
Centrum semiovale	15.1 ± 2.2	1.3 ± 0.3	0.39 ± 0.09	1.2 ± 0.3
Cerebral cortices	37.7 ± 5.3	2.8 ± 0.2	0.40 ± 0.07	3.0 ± 0.4

Values are shown as mean ± SD

Units are mL/100 mL/min, mL/100 mL, and mL/100 mL/min for CBF, CBV, and CMRO<sub>2</sub>, respectively

Significant differences between DIXON and DIXONbone without motion correction: \**P* < 0.001, <sup>†</sup>*P* < 0.01, <sup>‡</sup>*P* < 0.05

Significant differences between DIXON with and without motion correction: <sup>§</sup>*P* < 0.001, <sup>||</sup>*P* < 0.01, <sup>¶</sup>*P* < 0.05

Significant differences between DIXONbone with and without motion correction: <sup>\*\*</sup>*P* < 0.001, <sup>††</sup>*P* < 0.01

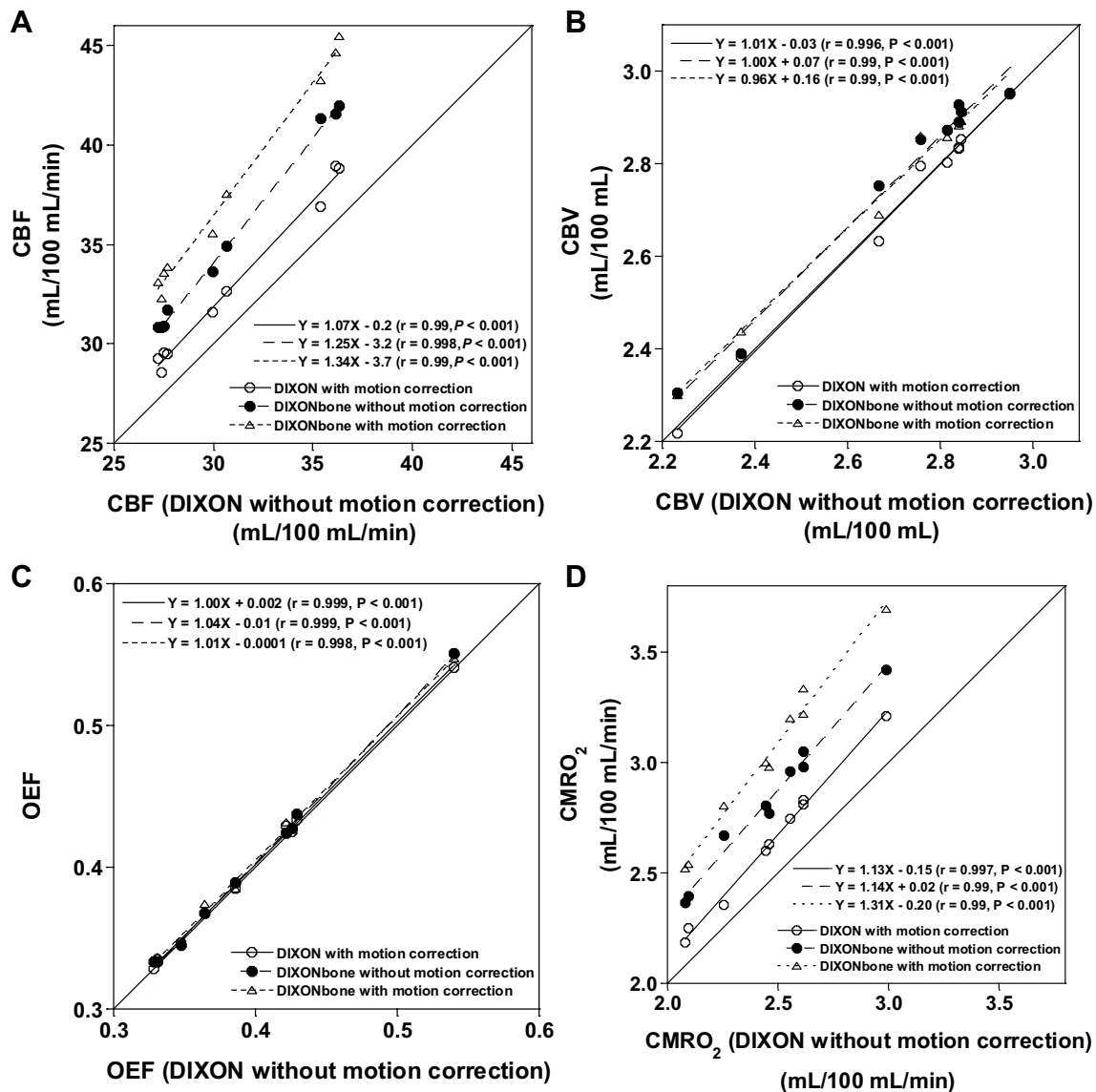


**Fig. 2** The relations of cerebral blood flow (CBF) (a), cerebral blood volume (CBV) (b), cerebral oxygen extraction fraction (OEF) (c) and cerebral metabolic rate of oxygen (CMRO<sub>2</sub>) (d) in the cerebral cortices of each subject between the values with attenuation correction by Dixon sequence (DIXON) without real-time motion correction and

values with attenuation correction by DIXON with real-time motion correction, or values with attenuation correction by Dixon sequence with model-based bone segmentation (DIXONbone) with or without real-time motion correction. Significant correlations are observed in all relations

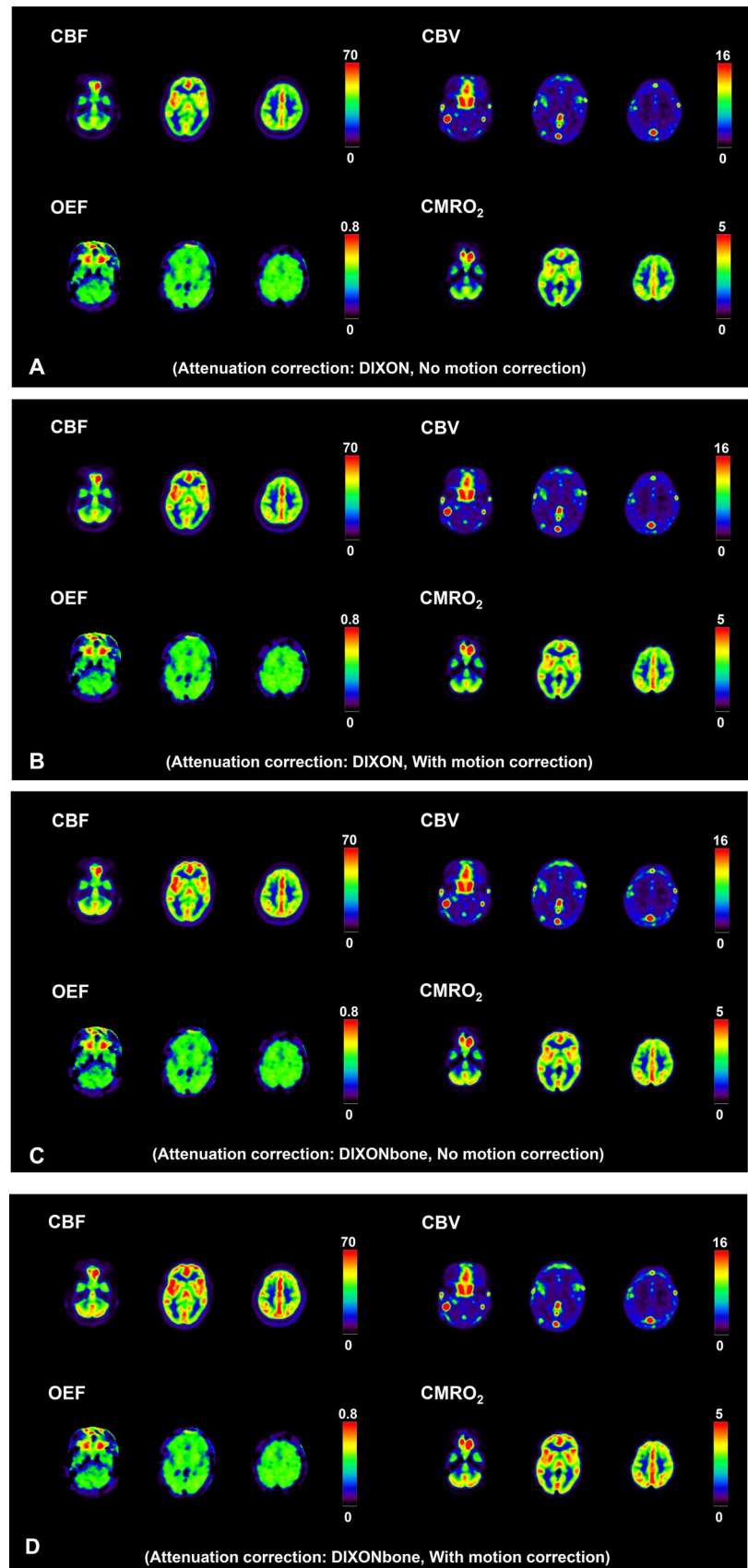
static magnetic field, non-magnetic medical devices were used for arterial blood sampling. Similar regional distributions of CBF, CBV, OEF, and CMRO<sub>2</sub> were obtained using a PET/MRI scanner as compared with those by PET alone scanner system reported previously [22].

The values of CBF, CBV, and CMRO<sub>2</sub> measured with attenuation correction by DIXON were significantly lower than those measured with correction by DIXONbone. One of the reasons for this is that attenuation correction of DIXON does not take into consideration of the photon absorption by bone [18, 23]. Since the values of CBF, CBV, and CMRO<sub>2</sub> includes scale factors to radioactivity concentration in brain,

these values might be affected by the attenuation correction methods. On the other hand, the values of OEF are relative values corresponding to ratios of CMRO<sub>2</sub> to CBF. Thus, OEF values were not affected by the attenuation correction methods.

The values of CBF and CMRO<sub>2</sub> with a real-time motion correction were slightly higher than those without correction. It has been reported that real-time motion corrected images with the present method showed about 10% large FWHM as compared with static images in phantom studies [21]. However, improving tissue mixture between gray and white matter and cerebrospinal fluid caused by

**Fig. 3** Typical PET images of cerebral blood flow (CBF), cerebral blood volume (CBV), cerebral oxygen extraction fraction (OEF) and cerebral metabolic rate of oxygen (CMRO<sub>2</sub>). **a** Attenuation correction is performed using Dixon sequence (DIXON). No real-time motion correction is performed. **b** Attenuation correction is performed using DIXON. A real-time motion correction is performed. **c** Attenuation correction is performed using Dixon sequence with model-based bone segmentation (DIXONbone). No real-time motion correction is performed. **D**: Attenuation correction is performed using DIXONbone. A real-time motion correction is performed. Scale maximum values are 70 mL/100 mL/min, 16 mL/100 mL, 0.8, and 5 mL/100 mL/min for CBF, CBV, OEF, and CMRO<sub>2</sub> images, respectively. The image slices are the same as Fig. 1



head movement using a real-time motion correction might introduce increasing values of CBF and CMRO<sub>2</sub>. Although head fixation during PET measurement often causes physical stress for patients, a real-time motion correction technique might realize the PET measurement without head fixation.

The coefficients of variation of CBF, CBV, OEF, and CMRO<sub>2</sub> in the cerebral cortices were almost the same among attenuation corrections by DIXON and DIXONbone with and without real-time motion correction. These coefficients of variation were almost the same as those previously reported, indicating the validity of measurement of CBF, CBV, OEF, and CMRO<sub>2</sub> using the PET/MRI scanner system [17, 22].

Using the PET/MRI scanner system with adequate corrections, similar values of CBF, CBV, OEF, and CMRO<sub>2</sub> with the PET alone scanner system reported previously were obtained [17, 22]. Measurement of CBF, CBV, OEF, and CMRO<sub>2</sub> using <sup>15</sup>O-labeled gases is useful for investigation of the pathophysiology of occlusive cerebrovascular disease, especially for assessment of the stage II hemodynamic compromise [1–7]. The PET/MRI scanner system can also be used for assessment of the stage II hemodynamic compromise.

The diffusion-weighted image (DWI) is a better imaging method to detect early ischemic lesions in stroke patients, and is widely used for clinical diagnosis of acute brain ischemia [24]. It has been reported that the area of cerebral infarction was slightly smaller than that of abnormality demonstrated by the DWI in the acute phase of brain ischemia in animal and human [25, 26]. Although the pathophysiology in such area showing discrepancy between the final area of cerebral infarction and the area of lesion detected by DWI is unknown, it can be investigated in relation to regional CMRO<sub>2</sub> using the PET/MRI scanner system with <sup>15</sup>O-labeled gases.

In conclusion, using the PET/MRI scanner system with the steady-state method of <sup>15</sup>O-labeled gases, CBF, CBV, OEF, and CMRO<sub>2</sub> could be measured. Values of CBF, CBV, and CMRO<sub>2</sub> measured with attenuation correction by DIXON were significantly lower than those measured with correction by DIXONbone. Values of CBF and CMRO<sub>2</sub> with real-time motion correction were slightly higher than those without correction. Using the PET/MRI scanner system with adequate corrections, similar values of CBF, CBV, OEF, and CMRO<sub>2</sub> with PET alone scanner system reported previously were obtained. PET/MRI scanner system can be used for assessment of the stage II hemodynamic compromise.

**Acknowledgements** This study was supported in part by a Grant-in-Aid for Scientific Research (C) (No. 16K10356) from the Japan Society for the Promotion of Science. We thank Mr. Yoshinobu Sato, Ms. Yayoi Kurihara, Mr. Minoru Oto, and Ms. Miho Aoki for their assistance in the PET experiments.

## Compliance with ethical standards

**Conflict of interest** The authors declare that they have no conflict of interest.

## References

- Gibbs JM, Wise RJ, Leenders KL, Jones T. Evaluation of cerebral perfusion reserve in patients with carotid-artery occlusion. *Lancet*. 1984;1:310–4.
- Powers WJ, Grubb RL, Raichle ME. Physiological responses to focal cerebral ischemia in humans. *Ann Neurol*. 1984;16:546–52.
- Powers WJ, Grubb RL, Darriet D, Raichle ME. Cerebral blood flow and cerebral metabolic rate of oxygen requirements for cerebral function and viability in humans. *J Cereb Blood Flow Metab*. 1985;5:600–8.
- Leblanc R, Yamamoto YL, Tyler JL, Diksic M, Hakim A. Borderzone ischemia. *Ann Neurol*. 1987;22:707–13.
- Kanno I, Uemura K, Higano S, Murakami M, Iida H, Miura S, et al. Oxygen extraction fraction at maximally vasodilated tissue in the ischemic brain estimated from the regional CO<sub>2</sub> responsiveness measured by positron emission tomography. *J Cereb Blood Flow Metab*. 1988;8:227–35.
- Sette G, Baron JC, Mazoyer B, Levasseur M, Pappata S, Crouzel C. Local brain haemodynamics and oxygen metabolism in cerebrovascular disease. Positron emission tomography. *Brain*. 1989;112:931–51.
- Yamauchi H, Fukuyama H, Kimura J, Konishi J, Kameyama M. Hemodynamics in internal carotid artery occlusion examined by positron emission tomography. *Stroke*. 1990;21:1400–6.
- Ogasawara K, Ito H, Sasoh M, Okuguchi T, Kobayashi M, Yukawa H, et al. Quantitative measurement of regional cerebrovascular reactivity to acetazolamide using <sup>123</sup>I-N-isopropyl-p-iodoamphetamine autoradiography with SPECT: validation study using H<sub>2</sub><sup>15</sup>O with PET. *J Nucl Med*. 2003;44:520–5.
- Ito H, Inoue K, Goto R, Kinomura S, Sato T, Kaneta T, et al. Error analysis of measured cerebral vascular response to acetazolamide stress by I-123-IMP autoradiographic method with single photon emission computed tomography: errors due to distribution volume of I-123-IMP. *Ann Nucl Med*. 2004;18:221–6.
- Derdeyn CP, Grubb RL Jr, Powers WJ. Cerebral hemodynamic impairment: methods of measurement and association with stroke risk. *Neurology*. 1999;53:251–9.
- Delso G, Ziegler S. PET/MRI system design. *Eur J Nucl Med Mol Imaging*. 2009;36:S86–92.
- Werner P, Barthel H, Drzezga A, Sabri O. Current status and future role of brain PET/MRI in clinical and research settings. *Eur J Nucl Med Mol Imaging*. 2015;42:512–26.
- Barthel H, Schroeter ML, Hoffmann KT, Sabri O. PET/MR in dementia and other neurodegenerative diseases. *Semin Nucl Med*. 2015;45:224–33.
- Delso G, Furst S, Jakoby B, Ladebeck R, Ganter C, Nekolla SG, et al. Performance measurements of the Siemens mMR integrated whole-body PET/MR scanner. *J Nucl Med*. 2011;52:1914–22.
- Watson CC, Newport D, Casey ME. A single scatter simulation technique for scatter correction in 3D PET. In: Grangeat P, Amans JL, editors. Three-dimensional image reconstruction in radiology and nuclear medicine. Dordrecht, The Netherlands: Kluwer Academic Publishers; 1996. p. 255–68.
- Frackowiak RS, Lenzi GL, Jones T, Heather JD. Quantitative measurement of regional cerebral blood flow and oxygen metabolism in man using <sup>15</sup>O and positron emission tomography:

- theory, procedure, and normal values. *J Comput Assist Tomogr.* 1980;4:727–36.
17. Ito H, Kanno I, Kato C, Sasaki T, Ishii K, Ouchi Y, et al. Database of normal human cerebral blood flow, cerebral blood volume, cerebral oxygen extraction fraction and cerebral metabolic rate of oxygen measured by positron emission tomography with <sup>15</sup>O-labelled carbon dioxide or water, carbon monoxide and oxygen: a multicentre study in Japan. *Eur J Nucl Med Mol Imaging.* 2004;31:635–43.
  18. Dickson JC, O'Meara C, Barnes A. A comparison of CT- and MR-based attenuation correction in neurological PET. *Eur J Nucl Med Mol Imaging.* 2014;41:1176–89.
  19. Koesters T, Friedman KP, Fenchel M, Zhan Y, Hermosillo G, Babb J, et al. Dixon sequence with superimposed model-based bone compartment provides highly accurate PET/MR attenuation correction of the brain. *J Nucl Med.* 2016;57:918–24.
  20. Catana C, Benner T, van der Kouwe A, Byars L, Hamm M, Chonde DB, et al. MRI-assisted PET motion correction for neurologic studies in an integrated MR-PET scanner. *J Nucl Med.* 2011;52:154–61.
  21. Inomata T, Watanuki S, Odagiri H, Nambu T, Karakatsanis NA, Ito H, et al. A systematic performance evaluation of head motion correction techniques for 3 commercial PET scanners using a reproducible experimental acquisition protocol. *Ann Nucl Med.* 2019;33:459–70.
  22. Yamaguchi T, Kanno I, Uemura K, Shishido F, Inugami A, Ogawa T, et al. Reduction in regional cerebral metabolic rate of oxygen during human aging. *Stroke.* 1986;17:1220–8.
  23. Ladefoged CN, Law I, Anazodo U, St Lawrence K, Izquierdo-Garcia D, Catana C, et al. A multi-centre evaluation of eleven clinically feasible brain PET/MRI attenuation correction techniques using a large cohort of patients. *Neuroimage.* 2017;147:346–59.
  24. van Everdingen KJ, van der Grond J, Kappelle LJ, Ramos LM, Mali WP. Diffusion-weighted magnetic resonance imaging in acute stroke. *Stroke.* 1998;29:1783–90.
  25. Minematsu K, Li L, Fisher M, Sotak CH, Davis MA, Fiandaca MS. Diffusion-weighted magnetic resonance imaging: rapid and quantitative detection of focal brain ischemia. *Neurology.* 1992;42:235–40.
  26. Yoneda Y, Tokui K, Hanihara T, Kitagaki H, Tabuchi M, Mori E. Diffusion-weighted magnetic resonance imaging: detection of ischemic injury 39 minutes after onset in a stroke patient. *Ann Neurol.* 1999;45:794–7.

**Publisher's Note** Springer Nature remains neutral with regard to jurisdictional claims in published maps and institutional affiliations.

## Authors and Affiliations

Hiroshi Ito<sup>1,2</sup> · Hitoshi Kubo<sup>2</sup> · Kazuhiro Takahashi<sup>2</sup> · Ken-Ichi Nishijima<sup>2</sup> · Naoyuki Ukon<sup>2</sup> · Ayaka Nemoto<sup>2</sup> · Shigeyasu Sugawara<sup>1,2</sup> · Ryo Yamakuni<sup>1</sup> · Masanobu Ibaraki<sup>3</sup> · Shiro Ishii<sup>1</sup>

<sup>1</sup> Department of Radiology and Nuclear Medicine, Fukushima Medical University, 1 Hikariga-oka, Fukushima 960-1295, Japan

<sup>2</sup> Advanced Clinical Research Center, Fukushima Medical University, Fukushima, Japan

<sup>3</sup> Department of Radiology and Nuclear Medicine, Akita Research Institute of Brain and Blood Vessels, Akita, Japan